JACS
JOURNAL OF THE AMERICAN CHEMICAL SOCIETY

Article

Facile Oxide to Chalcogenide Conversion for Actinides using the Boron-Chalcogen Mixture Method

Logan S Breton, Vladislav V. Klepov, and Hans-Conrad zur Loye

J. Am. Chem. Soc., **Just Accepted Manuscript** • DOI: 10.1021/jacs.0c06483 • Publication Date (Web): 26 Jul 2020

Facile Oxide to Chalcogenide Conversion for Actinides using the Boron-Chalcogen Mixture Method

Logan S. Breton,‡ Vladislav V. Klepov,‡* and Hans-Conrad zur Loye*

Department of Chemistry and Biochemistry, University of South Carolina, Columbia, SC, 29208

ABSTRACT: Actinide chalcogenides are of interest for fundamental studies of the behavior of 5*f* electrons in actinides located in a soft ligand coordination environment. As actinides exhibit an extremely high affinity for oxygen, the synthesis of phase pure actinide chalcogenide materials free of oxide impurities is a great challenge and, moreover, requires the availability and use of oxygen free starting materials. Herein, we report a new method, the Boron-Chalcogen Mixture (BCM) method, for the synthesis of phase pure uranium chalcogenides based on the use of a boron/chalcogen mixture, where boron functions as an "oxygen sponge" to remove oxygen from an oxide precursor and where the elemental chalcogen effects transformation of the oxide precursor into an oxygen free chalcogenide reagent. The boron oxide can be separated from the reaction mixture that is left to react to form the desired chalcogenide product. Several syntheses are presented that demonstrate the broad functionality of the technique and thermodynamic calculations that show the underlying driving force are discussed. Specifically, three classes of chalcogenides that include both new (rare earth uranium sulfides and alkali-thorium thiophosphates) and previously reported compounds were prepared to validate the approach: binary uranium and thorium sulfides, oxide to sulfide transformation in solid state reactions, and *in situ* generation of actinide chalcogenides in flux crystal growth reactions.

INTRODUCTION

Actinide chalcogenides adopt diverse structure types with distinct chemical compositions and specific actinide oxidation states,[1–6] which offer unique opportunities for studying 5*f* electron properties.[7–16] The synthesis of these materials can be achieved by a limited set of synthetic routes that include the traditional solid-state approach,[17–20] chemical vapor transport,[21–24] and the molten flux technique.[25–33] Regardless of the method chosen, there are two general actinide precursors that are consistently used – the actinide metals and binary actinide chalcogenides.[2, 34–38] One of the main obstacles faced when synthesizing the actinide chalcogenides are actinide oxide and oxychalcogenide impurities that often contaminate the resulting products and interfere with their property measurements.[39–41] Due to the high oxygen affinity of the actinides, even trace amounts of oxygen in the system will inevitably result in the formation of these impurities. Although careful oxygen exclusion from the reaction media is an intuitive and straightforward approach for avoiding oxide impurities, it is unfortunately often nearly impossible to completely eliminate oxide contamination present in the reagents themselves.[42, 43] This difficulty of needing to effectively deal with oxide or oxychalcogenide impurities in the starting materials motivated us to explore different synthetic approaches that would allow for the use of oxygen-contaminated reagents, or even oxides themselves, as the starting materials for the synthesis of oxygen free actinide chalcogenides.

In situations where oxygen cannot be avoided in the initial reagent mixture, it is reasonable to consider the use of a highly oxophilic sacrificial component that would extract oxygen and subsequently leave the reaction mixture or be dissolvable in post-reaction work-up. Aluminum powder with its high affinity for oxygen, in principle, would be a great candidate as an oxophilic component, however, its inertness, very high melting point (2072 °C) and low vapor pressure of the resulting Al_2O_3 makes its use inconvenient in typical reactions.[44] A better alternative is boron, which is almost as oxophilic as aluminum; however, it forms the much less inert B_2O_3 oxide. In fact, this approach has been successfully implemented in the sulfurization of some transition metal and rare earth oxides by incorporating a mixture of boron and sulfur into the reaction vessel.[45–50] The boron acts as an 'oxygen sponge' forming highly stable B_2O_3 while leaving the sulfur to replace oxygen. The success of the sulfurization is based on the differences between the formation energies of B_2O_3 ($\Delta_f G°$(vitreous-B_2O_3) = -1182.5 kJ/mol) and B_2S_3 ($\Delta_f G°$(vitreous-B_2S_3) = -247.6 kJ/mol), which strongly favors the formation of B_2O_3 thus leaving sulfur to react with the other reagents.[45] Despite the success with the rare earth and *d* elements, this approach has never been implemented for the synthesis of actinide chalcogenides. It is possible that this application was deemed unlikely to work for actinides due to their high oxophilicity and, thus, high stability of the actinide oxides. Thermodynamic calculations indicate, however, that this process should work for the actinides as well, which prompted us to investigate the effectiveness of using boron-chalcogen mixtures to achieve the formation of actinide chalcogenides when starting with actinide oxide precursors.[31]

Scheme 1. A schematic representation of the proposed method for the synthesis of actinide chalcogenides. Stable actinide oxides U_3O_8 and ThO_2 can be used as starting materials that are sulfurized to generate US_2 and ThS_2 as a final product or for *in situ* use in flux crystal growth and solid state reactions.

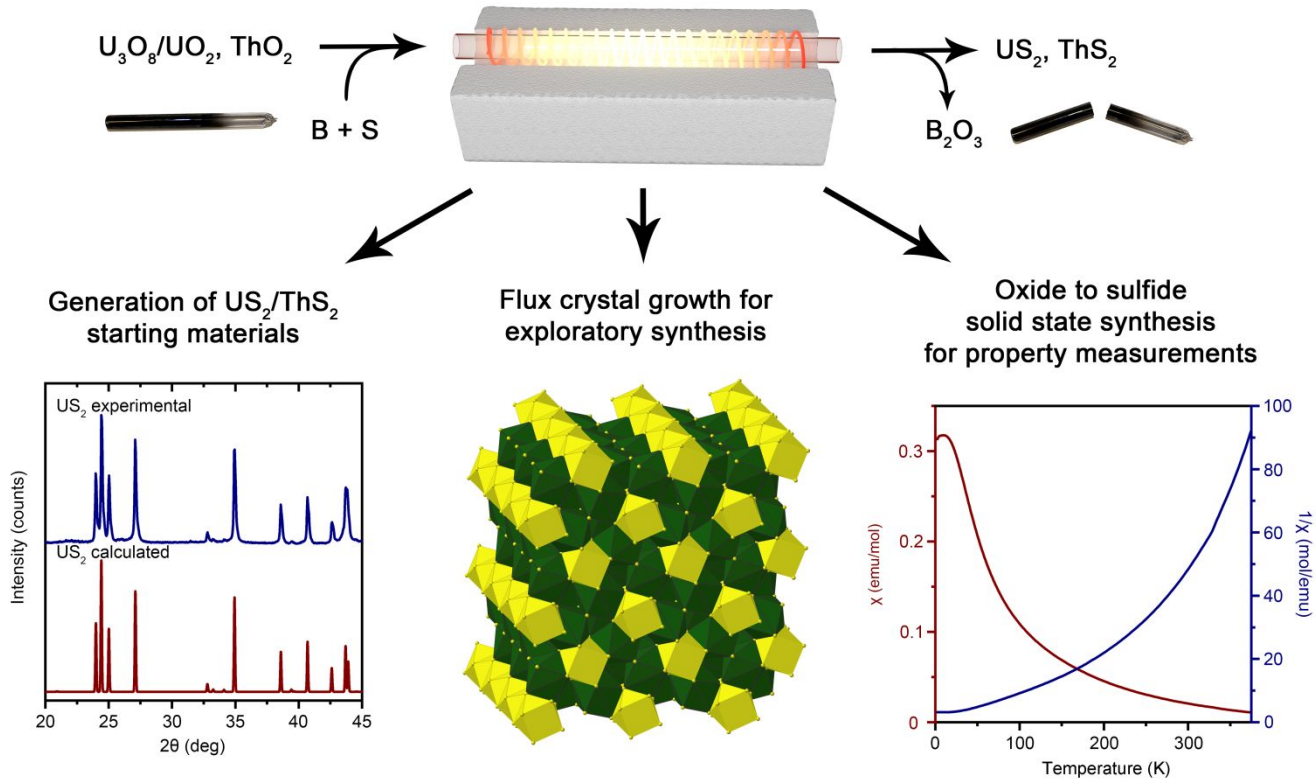

Herein we present the first time application of the boron-chalcogen mixture (BCM) method for the synthesis of actinide chalcogenides from their respective oxide precursors (Scheme 1). To demonstrate the efficacy of the BCM method, we present the synthesis of ThS_2 and US_2 starting from ThO_2 and U_3O_8, the solid state syntheses of U*M*S_3 (*M* = Ni and Co) perovskites starting with oxide reagents, the adaptation of the BCM method to flux crystal growth and the formation of the new family of rare earth uranium sulfides, $Ln_xU_2S_5$ (Ln = Pr, Nd, Sm, Gd-Yb) containing mixed valent U(III/IV), the crystal growth of the new complex thorium thiophosphate $Rb_{1.72}Na_{0.68}I_{0.40}[Th(PS_4)_2]$ using ThO_2 as a starting reagent, and the crystal growth of the uranium(V,VI) sulfide $Cs_6Cu_{12}U_2S_{15}$ obtained using the BCM method *in situ* generated polychalcogenide flux.[51] The single crystal structures and magnetic measurements of the new phases are presented. The new method will undoubtedly stimulate actinide chalcogenide research by bridging oxide and chalcogenide solid state chemistry and providing greatly improved access to phase pure chalcogenides and their properties.

RESULTS AND DISCUSSION

Proof of Concept: Binary actinide sulfides synthesis. To probe the feasibility of oxygen replacement by sulfur in uranium oxides, we treated UO_2 and U_3O_8 with a boron-sulfur (**B-S**) mixture in a carbon coated evacuated silica tube at 800 °C. As boron sulfides that form during the course of the reaction are corrosive in nature and can react with silica reaction vessels, it is necessary to heavily carbon coat the inside of the silica tubes to prevent corrosion and, ultimately, tube breakage. This is readily achieved by thermally decomposing acetone inside the empty silica tube at high temperatures.[45] The carbon coating prevents the tube from corroding and minimizes the introduction of possible contaminants in the product. The treatment of UO_2 and U_3O_8 with a B-S mixture resulted in a phase pure US_2 product with no detectable oxide or oxysulfide impurities by powder X-ray diffraction (Figure 1). This experiment proves that despite the uranium's high affinity for oxygen, it is possible to achieve full oxygen replacement by using the BCM method, suggesting the further extension of this method to other uranium chalcogenides as well as thorium analogues. To explore this extension of the BCM method, UO_2 and ThO_2 were reacted with boron-chalcogen mixtures (S, Se, Te) under identical reaction conditions. In all cases, except for the reaction between ThO_2 and a boron-tellurium mixture, was full oxygen replacement with chalcogens achieved. Moreover, the reactions with sulfur resulted in phase pure samples of US_2 and ThS_2 (Figure 1 and S1). We also found that the addition of an excess of the boron-chalcogen mixture results in the formation of polychalcogenide actinide compounds, a known class of chalcogenide materials.[52] Notably, even if an excess of boron is present, it does not incorporate into the reaction products. For the simple binaries, the reported method can find only a limited application for the synthesis of thorium tellurides as the only stable product that forms in the reactions between thorium ThO_2 and boron-tellurium mixtures is thorium oxytelluride, ThOTe.

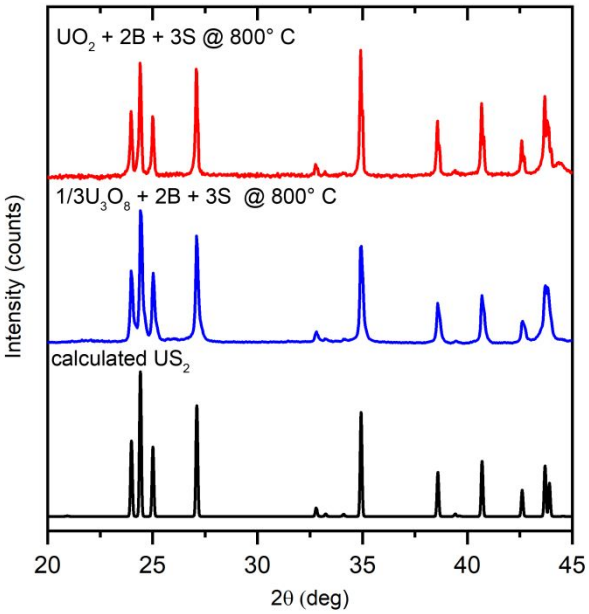

Figure 1. (top and middle) PXRD patterns of the products obtained from a reaction between UO_2 or U_3O_8 with B-S mixture at 800 °C and (bottom) calculated PXRD pattern of orthorhombic US_2.[53]

To probe the temperature dependence of the oxygen replacement with sulfur in oxides, we performed several reactions between U_3O_8/ThO_2 with a boron-sulfur (B-S) mixture (Figure S2 and S3). At low temperatures (below 500 °C) the B-S mixture reduces U_3O_8 to UO_2, with no indication of sulfide phase formation. The oxygen displacement by sulfur takes place between 500 and 600 °C, and full sulfurization finishes at temperatures below 700 °C, at which point all oxygen is fully replaced by sulfur to form US_2 and $U(IV)S_3$. The excess sulfur in US_3 sulfide-disulfide can be separated from the product by thermal decomposition at 800 °C, resulting in a phase pure US_2 or ThS_2 product for UO_2/U_3O_8 and ThO_2 stating materials, respectively.

Thermodynamic Stability. The observation of UOS and US_2 in the reactions at intermediate temperature suggests that there exist competing forces (kinetic and or thermodynamic) at these temperatures. In order to provide a thermodynamic basis for the observed experimental data, we calculated enthalpies of the reactions that form uranium and thorium compounds according to the following equations:

$UO_2/ThO_2 + 4/3\ B + nQ \rightleftharpoons UQ_n/ThQ_n + 2/3B_2O_3$ (1);

$\Delta H_r = \Delta_f H_{0\ K}(UQ_n/ThQ_n) + 2/3\Delta_f H_{0\ K}(B_2O_3) - \Delta_f H_{0\ K}(UO_2/ThO_2)$ (2);

$UO_2/ThO_2 + 1/3B + nQ \rightleftharpoons UOQ_n/ThOQ_n + 1/3B_2O_3$ (3);

$\Delta H_r = \Delta_f H_{0\ K}(UQ_n/ThQ_n) + 1/3\Delta_f H_{0\ K}(B_2O_3) - \Delta_f H_{0\ K}(UO_2/ThO_2)$ (4).

where Q is a chalcogen. Enthalpies of formation at 0 K for all compounds were taken from the OQMD database. [54, 55] As per equations (2) and (4) the energy cost of converting an oxide to a chalcogenide has to be compensated for by the energy gained when B_2O_3 is formed, as otherwise the reaction will not be energetically favorable. To compare the stability of different products, we plotted the

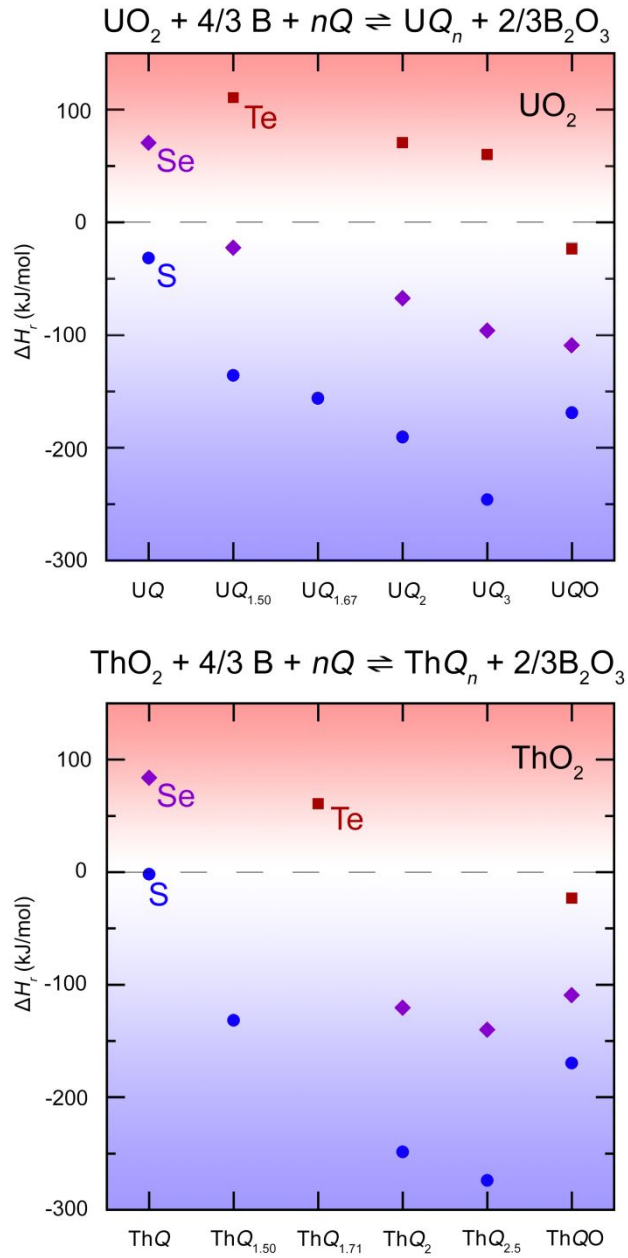

Figure 2. Enthalpies of formation of different uranium and thorium chalcogenide products in reaction (1) (for binary chalcogenides) and reaction (3) (for oxychalcogenides). $AnOQ$, AnQ_2 and AnQ_3 are among the most stable compounds in these systems. ΔH_r were estimated using calculated $\Delta_f H_{0\ K}$ values from The Open Quantum Materials Database.[54, 55]

calculated ΔH_r values in Figure 2. Although the entropies were not taken into account due to the lack of reliable literature values on these materials, the obtained enthalpic values are a good guide to overall phase stability and are in reasonable agreement with our experiments. For instance, in the U-O-S system, the addition of boron (and a respective change of the energy landscape in the system)[56] can result in the formation of binary chalcogenides US_3 and US_2, and an oxysulfide UOS, which are indeed observed among the products of a reaction between UO_2 and the B-S mixture. Between the two binaries, the most enthalpically favored is US_3, which forms at lower temperatures than US_2. As the temperature is increased, US_3 decomposes to US_2 and S, which is identical to the process occurring in a reaction between metal U and S, where US_3 can be formed at temperatures below ~ 600 °C followed by subsequent decomposition to US_2 and S at higher

temperatures.[57] Similar trends can be observed in the Se systems, where UQ_2 and UQ_3 are identified as the most stable compounds (Figure S4). The Te systems, however, are quite different from the S and Se ones in that only UOTe and ThOTe are predicted to have negative enthalpies of formation and therefore be stable. This is in good agreement with the experimental data for the Th-O-Te system, where only ThOTe was observed in the powder X-ray diffraction pattern. However, in the U-O-Te system, uranium forms a handful of telluride phases, most of which could not be identified unambiguously by PXRD but likely include polytelluride phases. Tellurium is known to have a greater ability to form polyanions compared to its sulfur and selenium congeners,[58] which could possibly give rise to additional factors not considered in the calculations and which could be the cause of the discrepancy. One can thus conclude that these predictions can be readily used when targeting specific sulfides and selenides, while targeting the telluride phases may require additional experimentation.

Overall, these experiments and thermodynamic findings provide evidence that the BCM method is an efficient and very convenient way for obtaining actinide chalcogenide and polychalcogenide precursors. Given the achieved success, it was decided to explore how generally applicable this method is and, thus, to apply this method to an *in situ* uranium chalcogenide generation in conventional solid state and flux reactions. As our interest lies in the magnetism of sulfide phases and their structural complexity, we focused mostly on the phases with magnetic ions and those that have the potential to exhibit a complex structure.

Solid state reactions using the BCM method. To date, solid state approaches for obtaining chalcogenide phases often involve the high temperature reaction of the respective elements. To probe the applicability of the BCM method for solid state reactions using oxides as starting materials, we selected $UNiS_3$ and $UCoS_3$ perovskites as target phases.[59] These compositions are of interest for a number of reasons including a +4 cation on the A site, interesting magnetic properties, and past difficulty in preparing a phase pure sample, (Figure 3).[60] To generate the target phases, we performed a series of two-step solid state reactions. In the first step, the precursors U_3O_8, NiO, and $CoC_2O_4{\cdot}2H_2O$ were weighed out in the proper stoichiometric quantities, pelletized, and pre-reacted at 1100 °C in air. As $NiUO_4$ forms only under high pressure,[61] we observed the formation of a mixture of NiO and U_3O_8 for the Ni-containing system, whereas the reaction with Co resulted in a pure $CoUO_4$ uranate (Figure S5). In the second step, the intermediate products were ground with a slight excess of the B-S mixture, pelletized, and reacted in an evacuated carbon-coated silica tube. We found that pure $UNiS_3$ forms at 850 °C, while the formation of $UCoS_3$ is not observed until a significantly higher temperature, 1100 °C, in agreement with the previous report.[59] The PXRD data confirm the formation of phase-pure, well crystalline products (Figure S6 and S7). Pure $UNiS_3$ also formed in a direct reaction between NiO, U_3O_8, and the B-S mixture, circumventing the intermediate step. These experiments demonstrate the major advantage of the BCM method, namely that air stable oxides can be used as starting materials to obtain phase pure chalcogenide target phases, including those that are extremely sensitive to the presence of oxygen in the system. In fact, the B-S mixture bridges oxide and sulfide solid state chemistry as it allows for oxygen replacement in virtually any oxide material and its potential for the synthesis of sulfide phases can hardly be overestimated.

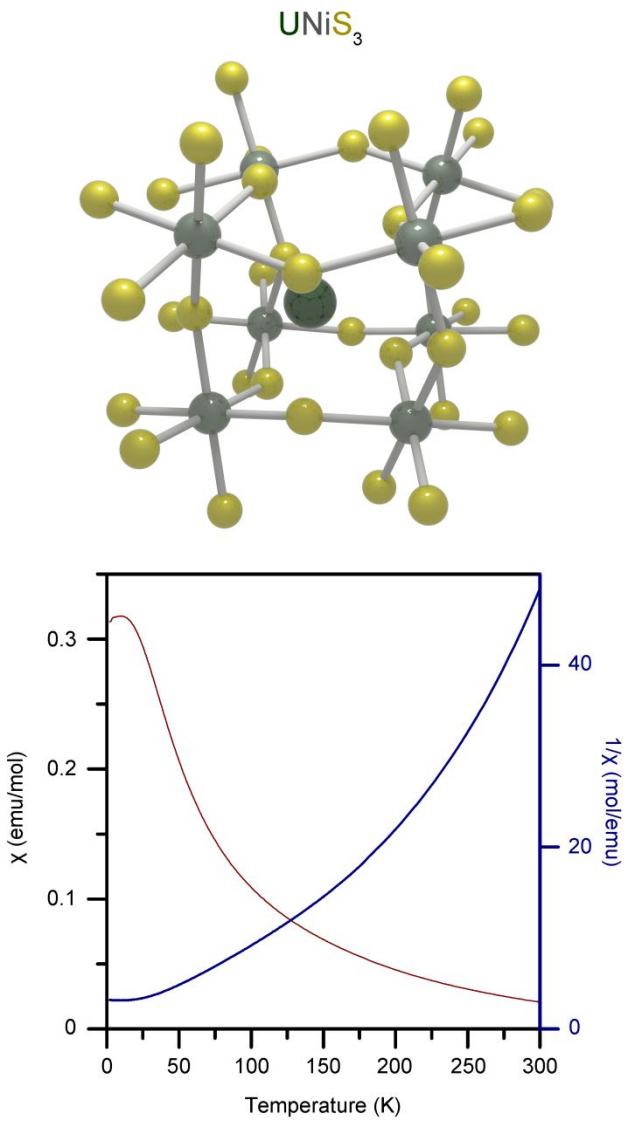

Figure 3. (top) Schematic of the orthorhombically distorted perovskite structure of $UNiS_3$ with U (dark-grey) and Ni(light grey) cations on the A and B sites, respectively, and (bottom) the magnetic susceptibility vs. temperature plot for $UNiS_3$.

The successful synthesis of $UCoS_3$ and $UNiS_3$ from an oxide using the BCM method allowed us to study their magnetic properties. As the magnetism of $UCoS_3$ has been reported before, we used it as a reference point, whereas the magnetic properties of $UNiS_3$ are reported here for the first time. As expected, the magnetic susceptibility of $UCoS_3$ in a range of 2 to 130 K falls in line with the previously reported data, [62] and exhibits a single magnetic transition at ~60 K, which is followed by a significant increase in the magnetic susceptibility, indicating a ferro- or ferrimagnetic transition (Figure S8). Unlike its Co analog, the magnetic susceptibility of $UNiS_3$ exhibits a downturn in the magnetic susceptibility at about 30 K (Figure 3). There is no indication of impurities in the PXRD patterns of the sample; moreover, we prepared samples that contain U and Ni in 0.98:1 and 1:0.98 molar ratios to account for possible impurities that could result from off-stoichiometry in the reagent mixture. As both samples showed the same magnetic behavior, one can surmise that this magnetic behavior is attributable to $UNiS_3$ rather than to an unidentified impurity. A magnetization vs. magnetic field plot collected from a fresh sample at room temperature showed that the sample acquires a

residual magnetization when exposed to a magnetic field (Figure S9). This fact indicates that there is some degree of glassy behavior in $UNiS_3$ at 300 K. We collected magnetic susceptibility up to 375 K but no clear magnetic transition was revealed. Additional studies using neutron diffraction to learn about potential magnetic order in $UNiS_3$ are planned for the future.

Flux crystal growth using the BCM method. **Successful synthesis of the $Ln_xU_2S_5$ series.** Flux crystal growth is one of the pillars of modern solid state chemistry that has functioned very efficiently for obtaining and characterizing new phases in single crystal form.[3, 63] Due to our interest in the magnetism of uranium sulfides, we investigated the rare earth uranium sulfide system to study the magnetic behavior and identify possible magnetic interactions between 4*f* and 5*f* orbitals.[64] Prior to realizing the potential use of the BCM method, we had synthesized several compounds in the $Ln_xU_2S_5$ series (*Ln* = Pr, Nd, Sm, Gd, Tb, and Dy, x = 0.70–0.89) using US_2 as a starting material. Unfortunately, the majority of the reaction products were contaminated by UOS as a result of the hygroscopic nature of US_2[44, 65]. We decided to reinvestigate this system using the BCM method to study the method's effectiveness in flux crystal growth reactions.

To eliminate oxygen from the system and to obtain the target $Ln_xU_2S_5$ products, a series of reactions using UO_2 and Ln_2S_3 with the B-S mixture were performed in evacuated carbon-coated silica tubes. This resulted in the successful synthesis of the $Ln_xU_2S_5$ series without oxygen impurities. Moreover, we attempted reactions targeting the compositions that previously did not form when US_2 was used as a starting material; this led to phase pure single crystalline samples of $Ln_xU_2S_5$ with *Ln* = Ho, Tm, and Yb. In all cases, a white opaque layer of, presumably, B_2O_3 could be seen attached to the exposed silica at the top of each tube; the final $Ln_xU_2S_5$ products did not contain oxide impurities as determined by PXRD. Magnetic measurements were performed on phase pure samples of $Ln_xU_2S_5$ with *Ln* = Tb, Dy, Ho, Er, Tm, and Yb, (Figure S10-S15), to show their paramagnetic behavior down to 2 K, Figures (S16-S21). Although the Curie-Weiss law fits allowed us to derive the magnetic moments of these compounds (Table S1), the exact lanthanide content varies slightly between crystals, thereby affecting the exact U(III) to U(IV) ratio, making an assignment of magnetic moments to specific species in the structures not possible. Similar issues were observed in the previously reported isotypic material $U_{1+\delta}S_2$ that also contains uranium in the +3 and +4 oxidation states, the ratio of which is a function of δ.[66]

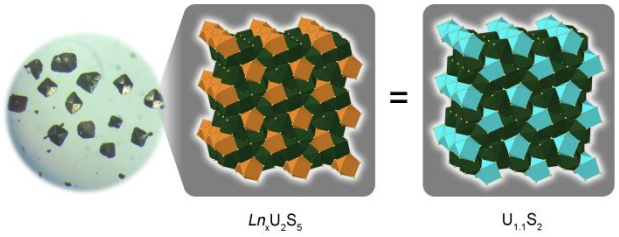

Figure 4. (left) An optical image of single crystals of the Nd analogue of the $Ln_xU_2S_5$ series along with a comparison of the (middle) $Ln_xU_2S_5$ structure with (right) that of the presumed parent structure, $U_{1.1}S_2$.

Thorium thiophosphates. The successful synthesis of the $Ln_xU_2S_5$ series demonstrated the use of the BCM method for the crystal growth of rare earth uranium sulfides. To see if this approach could be extended to other actinides, we utilized the BCM method for the crystal growth of thorium containing chalcogenides. We targeted a thorium analog of previously reported uranium thiophosphates with complex topology and relatively large unit cells (>7,500 Å^3).[67] The use of a RbI flux with the BCM method for *in situ* sulfurization of ThO_2 in the presence of P_2S_5 and Na_2S resulted in the formation of single crystals of $Rb_{1.72}Na_{0.68}I_{0.40}[Th(PS_4)_2]$, a close analog of previously reported $Rb_{1.35}Na_{0.93}I_{0.28}[U(PS_4)_2]$ that was obtained via a normal flux crystal growth reaction using US_2 as a starting reagent.

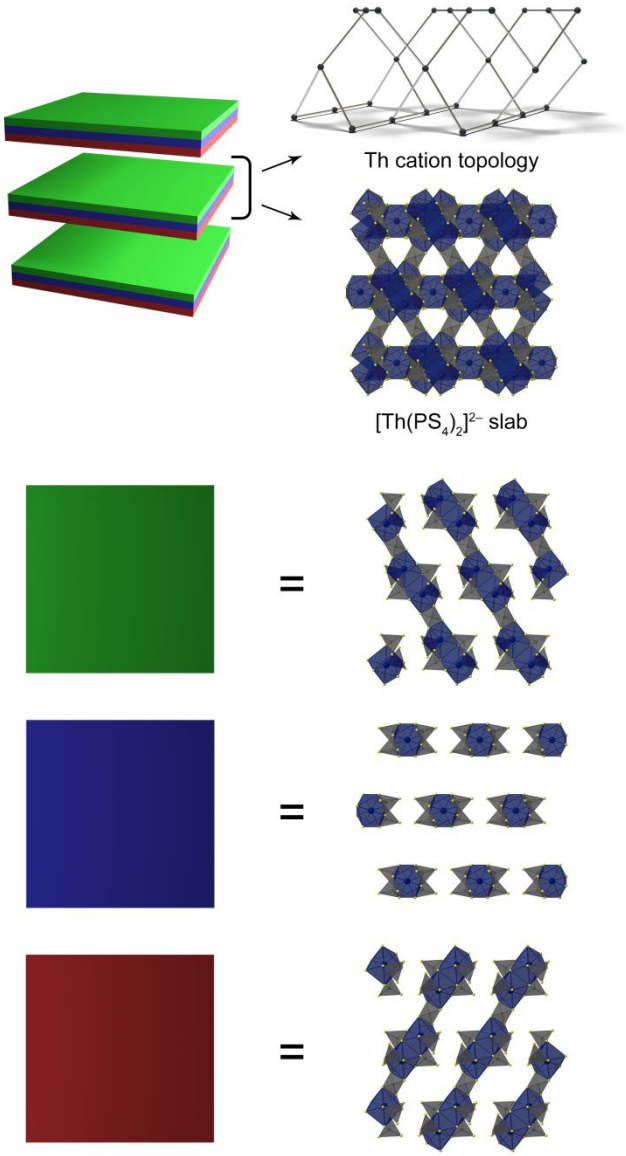

Figure 5. A schematic representation of the $Rb_{1.72}Na_{0.68}I_{0.40}[Th(PS_4)_2]$ structure. The main structural unit is a $[Th(PS_4)_2]^{2-}$ slab that consists of three pseudo-layers (shown as green, blue, and red plates). The slabs are filled with disordered Rb^+, Na^+, and I^- ions, maintaining its charge balance.

The new thorium compound synthesized using the BCM method is composed of $[Th(PS_4)_2]^{2-}$ slabs, identical to their $[U(PS_4)_2]^{2-}$ analogs, that are filled with severely disordered Na^+, Rb^+, and I^- ions (Figure 5). While uranium compounds comprise the majority of the reported actinide sulfides (253 entries in ICSD), thorium sulfides are significantly less

common with only 55 entries.[68–71] The small number of reported thorium analogs can potentially be attributed to their perceived similarity to the uranium counterparts and therefore a lack of interest in their synthesis that many would consider redundant.[17] However, the synthesis of the thorium analogs of uranium compounds can be beneficial as it is sometimes difficult to determine the oxidation state of uranium based solely on crystallographic data; while uranium has a range of oxidation states from +2 to +6 in its sulfides,[72–77] thorium does not adopt an oxidation state higher than +4. Therefore, introduction of this simple and effective synthetic method for thorium sulfides can help clarify uranium oxidation states in chalcogenide systems and lead to a significant boost in the number of reported thorium sulfides in the future.

Application of the BCM method for the synthesis of U(V,VI) chalcogenides. There are only few reports on uranium sulfides with uranium in oxidation states higher than +4, as the chalcogenides tend to stabilize uranium in oxidation states lower than +5. There are a few exceptions, such as the series of alkali copper uranium sulfides, $M_6Cu_{12}U_2S_{15}$ (M = K, Rb, Cs), in which uranium exhibits the formal oxidation state of +6, although there is experimental evidence of U(V) admixture in these compounds.[49] In order to probe the potential of the new BCM method for the formation of uranium sulfides in uncommon oxidation states, the synthesis of $Cs_6Cu_{12}U_2S_{15}$ was targeted by replacing U metal with U_3O_8 as a starting material. Moreover, we replaced Cs_2S (in the original synthesis) that generated a polychalcogenide flux with Cs_2CO_3 and an additional quantity of the B-S mixture to generate the flux *in situ* from a commercially available carbonate. In doing so, all air- and moisture-sensitive chalcogenide starting materials were replaced with ones that can be handled in air, i.e. U_3O_8, Cu, Cs_2CO_3, B, and S, circumventing the need of using inert atmospheres (e.g. a glovebox or a glovebag) and greatly simplifying reaction preparation. This process resulted in the successful synthesis of the target phase, as confirmed by SC XRD and powder XRD analysis. This experiment concludes a full range of actinide sulfide materials can be targeted using this new method.

CONCLUSION

In summary, we demonstrated the first successful application of the BCM method for a full range of actinide chalcogenide syntheses, including binary actinide chalcogenide syntheses, solid state synthesis and flux crystal growth reactions. An unprecedented one-step transformation of the stable U_3O_8 and ThO_2 actinide oxides to phase pure US_2 and ThS_2 was achieved at 800 °C. Solid state sulfurization reactions were developed to demonstrate oxygen replacement in a NiO + U_3O_8 mixture, and $CoUO_4$, to form $UNiS_3$ and $UCoS_3$ perovskites, respectively, the magnetic properties of which are reported. Further development of solid state sulfurization reactions is of paramount importance for actinide chalcogenide chemistry as it bridges oxide and chalcogenide solid state chemistry, opening a new synthetic route toward actinide chalcogenides.

To demonstrate the applicability of this method for exploratory flux crystal growth, a wide range of actinide chalcogenides with different fluxes were synthesized, particularly, a new family of mixed 4*f*/5*f* compounds $Ln_xU_2S_5$ in a CsCl flux, a thorium thiophosphate with complex topology $Rb_{1.72}Na_{0.68}I_{0.40}[Th(PS_4)_2]$ in a RbI flux, and a U(V,VI) sulfide $Cs_6Cu_{12}U_2S_{15}$ in an *in situ* generated polysulfide flux. One great advantage of this method is that it allows for actinide chalcogenide generation at relatively low temperatures, below 600 °C, allowing for the use of polychalcogenide fluxes. We believe that the combination of convenient exploratory crystal growth and an easy solid state route toward phase pure materials, which is necessity for property measurements, creates a synergy that will significantly boost research in the field of actinide chalcogenides.

EXPERIMENTAL SECTION

Caution! Both thorium and uranium, although the uranium precursor used in this synthesis contains depleted uranium, require that proper procedures for handling radioactive materials are observed. All handling of radioactive materials was performed in laboratories specially designated for the study of radioactive actinide materials.

General considerations. All reagents were obtained from commercial sources and were used without further purification. All reactions with chalcogens were carried out in carbon-coated fused silica tubes (10×12mm inner and outer diameters, about 12 cm length). All reagents were handled in air, except for P_2S_5 and Na_2S, which were handled in a nitrogen filled glovebag. Phase composition of all products was determined by powder X-ray diffraction using a Bruker D2 Phaser instrument. Magnetic property measurements were performed using a Quantum Design MPMS 3 SQUID magnetometer. Single-crystal X-ray diffraction data were collected at 300(2) K on a Bruker D8 QUEST diffractometer equipped with an Incoatec IμS 3.0 microfocus radiation source (MoKα, λ = 0.71073 Å) and a PHOTON II area detector (Tables S2-S16). Quantitative elemental analysis was performed on product single crystals using a Tescan Vega-3 SEM instrument equipped with a Thermo EDS attachment (Table S17 and Figures S22-S33).

Chalcogenation reactions. The reactions between actinide oxides AnO_2 (An = U and Th) and chalcogens were studied at 800 °C using 1:2:3 and 1:4:6 molar ratios of the starting materials AnO_2, B, and Q (Q = S, Se, Te); and were sulfurized at different temperatures (400, 500, 600, 700, and 800 °C) using 1:6:9 and 1:2:3 molar ratios for U_3O_8:B:S and ThO_2:B:S, respectively (see Tables S18 and S19 for detailed information). All reactions were placed into a programmable furnace, ramped up to the desired temperature, where it was held for 24 hours. The phase composition of the products was determined by PXRD. It is important to note that in principle boron can act as a reducing agent toward the other reagents. In practice it appears that the stability of the product phase also significantly influences the actinide oxidation state in the syntheses described.

Uranium Lanthanide Sulfides, $Ln_xU_2S_5$. For Ln = Pr-Dy, a 6:1 molar ratio of US_2 and Ln_2S_3 respectively was used along with 1 gram of CsCl flux. For Ln = Ho-Yb, a 1:1:6:9 molar ratio of UO_2, Ln_2S_3, B, and S, respectively, was used along with 1 gram of CsCl flux. All reactions were put in a programmable furnace and ramped up to 400 °C in 1 hour, then slowly ramped at 20 °C/hour to 750 °C where it was held for 20 hours. The furnace was then cooled to 550 °C at a rate of 8 °C/hour and subsequently shut down to cool to room temperature. The product was sonicated in water to dissolve and remove the CsCl flux from the desired product. After sonication, the water was decanted off the product, and the product was vacuum filtered, washed with water and acetone, and dried in air.

$UNiS_3$ was obtained in a solid state reaction between 0.1127 g of U_3O_8 and 0.030 g of NiO in a 1:3 molar ratio with 0.0631 g of B-S mixture (9% excess) with a 2:3 B:S molar ratio. The mixture was thoroughly ground and pelletized before reacting it at 850 °C for 12 h. **$UCoS_3$** was obtained from $CoUO_4$ that resulted from a reaction between $CoC_2O_4{\cdot}2H_2O$ and U_3O_8 in a 3:1 molar ratio at 1100 °C. After confirming phase purity by PXRD, $CoUO_4$ (0.0861 g) was ground with 0.0382 g of the B-S mixture (2% excess based on O content) and reacted at 1100 °C for 3 h. The phase purity of the obtained $UCoS_3$ was confirmed by PXRD.

$Rb_{1.72}Na_{0.68}I_{0.40}[Th(PS_4)_2]$ was obtained in a flux crystal growth reaction between ThO_2, Na_2S, P_2S_5, B, and S in a 1:4:4:4:6 ratio (based on 0.0874 g of ThO_2) with 1.0 g of a RbI flux. The reaction was ramped up to 720 °C in 1 h, dwelled for 10 h, and cooled to 500 °C at a 10 °C/h rate. The product was separated from the flux by dissolving the flux in 30 mL of DMF and filtering using vacuum filtration. While the obtained transparent crystals are somewhat moisture sensitive, they rapidly react with liquid water releasing H_2S.

$Cs_6Cu_{12}U_2S_{15}$ was obtained in a reaction between U_3O_8, Cu, Cs_2CO_3, B, and S in a 1:12:8:30 ratio. Due to hygroscopic nature of Cs_2CO_3, it was dried in an oven overnight at 260 °C. The reaction was ramped up to 600 °C at a 50 °C/h rate, dwelled for 24 h, and cooled to 200 °C in 40 h. The product was separated from the formed polychalcogenide flux by dissolving the flux in several portions (about 30 mL each) of DMF. Black blocks of the target phase formed along with other unidentified phases. Structure determination from single crystal X-ray diffraction unambiguously confirmed the identity of the crystal (Table S4).

Crystal structure description. ***Ln*$_x$U$_2$S$_5$** crystallizes in the *P*4/*ncc* space group and consists of edge sharing US_8 distorted bicapped trigonal prisms with channels that are filled with highly disordered face sharing *Ln*S_8 square antiprisms (Figure S34). The U–S bond lengths range from 2.7319(2) to 2.9982(9) Å and the *Ln*–S bond lengths range from 2.674(5) to 2.994(6) Å. The disorder of the lanthanide cations within the channels result in the nonstoichiometric formula, Ln_xUS_5. The occupancy of the lanthanide was found to be dependent on its nature, generally slightly decreasing along the lanthanide series. The obtained structures are closely reminiscent with the structure of α-"US_2" with a composition of $U_{1.1}S_2$. A comparison of the $U_{1.1}S_2$ structure with that of the $Ln_xU_2S_5$ series (Figure 4) suggests that the lanthanide cations replace the US_8 square antiprisms within the $U_{1.1}S_2$ parent structure. Given that uranium has a valency of +3.6 in $U_{1.1}S_2$, which implies mixed +3/+4 valency of the U cations in the structure, one can surmise that a mixed uranium valency is observed in the $Ln_xU_2S_5$ series. [66] Bond valence sums were calculated by using the U–S distances in each analogue along with R_0 and B values of 2.55 and 0.37, respectively,[78] and show an average uranium oxidation state of 3.76, supporting the presence of an admixture of U(III)/U(IV) on the uranium sites (Table S20).

$Rb_{1.72}Na_{0.68}I_{0.40}[Th(PS_4)_2]$ crystallizes in the *Ccce* space group and forms a structure that is an analogue of the previously reported $Rb_{1.35}Na_{0.93}I_{0.28}[U(PS_4)_2]$. In the structure of $Rb_{1.72}Na_{0.68}I_{0.40}[Th(PS_4)_2]$, the thorium atoms are each surrounded by 8 sulfur atoms forming trigonal dodecahedra with Th–S bond lengths of 2.813(2)–3.0392(19) Å. The phosphorus atoms form PS_4^{3-} thiophosphate tetrahedra with P–S bond lengths of 1.977(3)–2.078(3) Å (average 2.034(9) Å) and S–P–S angles ranging from 103.9(12)—113.9(17)° (average 109.5°). The complex structure of $Rb_{1.72}Na_{0.68}I_{0.40}[Th(PS_4)_2]$ is comprised of $[Th(PS_4)_2]^{2-}$ slabs held together by severely disordered Rb^+, Na^+, and I^- ions, which are located both between the slabs as well as through the pores within the slabs. Each individual slab can be dissected into three separate layers; a bottom, middle, and top layer (Figure 5). The bottom and top layers are both composed of parallel $[Th(PS_4)_2]^{2-}$ chains but differ in that the top layer is mirrored and rotated 60° relative to the bottom layer. These two layers are then connected through the middle layer which is composed of $Th(PS_4)_4$ groups which connect two chains in the top layer and two chains in the bottom layer.

ASSOCIATED CONTENT

PXRD patterns, structure figures, magnetic plots, SEM images and spectra, BVS table, crystallographic tables (PDF). This material is available free of charge via the Internet at http://pubs.acs.org. CSD 2009876- 2009886, 1962605 contain the supplementary crystallographic data for this paper. The data can be obtained free of charge from The Cambridge Crystallographic Data Centre via www.ccdc.cam.ac.uk/structures.

AUTHOR INFORMATION

Corresponding Authors

Hans-Conrad zur Loye; Email: *zurloye@mailbox.sc.edu*

Vladislav V. Klepov; Email: *vladislavklepov@gmail.com*

Author Contributions

‡These authors contributed equally.

Notes

The authors declare no competing financial interest.

ACKNOWLEDGMENT

Research supported by the US Department of Energy, Office of Basic Energy Sciences, Division of Materials Sciences and Engineering under award DE-SC0018739.

REFERENCES

(1) Mesbah, A.; Prakash, J.; Ibers, J. A. Overview of the crystal chemistry of the actinide chalcogenides: incorporation of the alkaline-earth elements, *Dalton Trans.*, **2016**, *45*, 16067-16080.

(2) Bugaris, D. E.; Ibers, J. A. Synthesis and characterization of some solid-state actinide (Th, U, Np) compounds, *Dalton Trans.*, **2010**, *39*, 5949-5964.

(3) Kanatzidis, M. G. Discovery-Synthesis, Design, and Prediction of Chalcogenide Phases, *Inorg. Chem.*, **2017**, *56*, 3158-3173.

(4) Choi, K.-S.; Kanatzidis, M. G. New Uranium Chalcoantimonates, RbU_2SbS_8 and KU_2SbSe_8, with a Polar Noncentrosymmetric Structure, *Chem. Mater.*, **1999**, *11*, 2613-2618.

(5) Chondroudis, K.; Kanatzidis, M. G. Stabilization of U^{5+}in $Rb_4U_4P_4Se_{26}$. An Actinide Compound with a Mixed Selenophosphate/Polyselenide Framework and Ion-Exchange Properties, *J. Am. Chem. Soc.*, **1997**, *119*, 2574-2575.

(6) Prakash, J.; Mesbah, A.; Beard, J. C.; Lebegue, S.; Malliakas, C. D.; Ibers, J. A. Synthesis, crystal structure, optical, and electronic study of the new ternary thorium selenide $Ba_3ThSe_3(Se_2)_2$, *J. Solid State Chem.*, **2015**, *231*, 163-168.

(7) Wang, S.; Alekseev, E. V.; Depmeier, W.; Albrecht-Schmitt, T. E. Recent progress in actinide borate chemistry, *ChemComm*, **2011**, *47*, 10874.

(8) Krivovichev, S. V.; Burns, P. C.; Tananaev, I. G.; *Structural Chemistry of Inorganic Actinide Compounds*; Elsevier Science, **2007**.

(9) Jayasinghe, A. S.; Lai, Y.; Baumbach, R.; Latturner, S. E. $U_{1.33}T_4Al_8Si_2$ (T = Ni, Co): Complex Uranium Silicides Grown from Aluminum/Gallium Flux Mixtures, *Inorg. Chem.*, **2019**, *58*, 12209-12217.

(10) Li, Y.; Yang, Z.; Wang, Y.; Bai, Z.; Zheng, T.; Dai, X.; Liu, S.; Gui, D.; Liu, W.; Chen, M.; Chen, L.; Diwu, J.; Zhu, L.; Zhou, R.; Chai, Z.; Albrecht-Schmitt, T. E.; Wang, S. A mesoporous cationic thorium-organic framework that rapidly traps anionic persistent organic pollutants., *Nat. Commun.*, **2017**, *8*, 1354.

(11) Manos, E.; Kanatzidis, M. G.; Ibers, J. A. Actinide Chalcogenide Compounds. In *The Chemistry of the Actinide and Transactinide Elements*: Morss, L. R., Edelstein, N. M., Fuger, J., Eds.; Springer: Dordrecht, **2010**; pp 4005-4077.

(12) Wickleder, M. S.; Fourest, B.; Dorhout, P. K. Thorium. In *The Chemistry of the Actinide and Transactinide Elements*: Morss, L. R., Edelstein, N. M., Fuger, J., Eds.; Springer: Dordrecht, **2008**; pp 95-97.

(13) Grenthe, I.; Drozdzynski, J.; Fujino, T.; Buck, E. C.; Albrecht-Schmitt, T. E.; Wolf, S. F. Uranium. In *The Chemistry of the Actinide and Transactinide Elements*: Morss, L. R., Edelstein, N. M., Fuger, J., Eds.; Springer: Dordrecht, **2008**; pp 412-420.

(14) Mar, A.; Tougait, O.;, M. P. H. N.; Lopes, E. B. Anisotropic Transport and Magnetic Properties of Ternary Uranium Antimonides U_3ScSb_5 and U_3TiSb_5, *Chem. Mater.*, **2006**, *18*, 4533-4540.

(15) Kindra, D. R.; Evans, W. J. Magnetic Susceptibility of Uranium Complexes, *Chem. Rev.*, **2014**, *114*, 8865-8882.

(16) Freeman, A. J. f-Electrons in solids: Electronic structure and properties of actinides and rare-earths, *Physica B+C*, **1980**, *102*, 3-11.

(17) Narducci, A. A.; Ibers, J. A. Ternary and Quaternary Uranium and Thorium Chalcogenides, *Chem. Mater.*, **1998**, *10*, 2811-2823.

(18) Noel, H. Chimie Minerale — Combinaisons seleniees de l'uranium dans les systemes USe_2-MSe (M = Mg, Ti, V, Cr, Mn, Fe, Co, Ni), *C. R. Acad. Sc. Paris*, **1974**, *279*, 513-515.

(19) Yao, J.; Ibers, J. A. $Ba_4Cr_2US_9$: The First Chalcogenide Analogue of the Perovskite-related $(A_3A'BO_6)_m(A_3B_3O_9)_n$, *Z. Anorg. Allg. Chem.*, **2008**, *634*, 1645-1647.

(20) Narducci, A. A.; Ibers, J. A. The related compounds $MThTe_3$ (M = Mn, Mg) and $ACuThSe_3$ (A = K, Cs): Syntheses and Characterization., *Inorg. Chem.*, **2000**, *39*, 688-691.

(21) Daoudi, A.; Lamire, M.; Levet, J. C.; Noel, H. New Ternary Uranium Copper Chalcogenides $Cu_2U_3S_7$ and $Cu_2U_3Se_7$: Crystal

Structure and Magnetic Properties, *J. Solid State Chem.*, **1996**, *123*, 331-336.

(22) Bugaris, D. E.; Ibers, J. A. Synthesis, structures, and magnetic and optical properties of the compounds $[Hg_3Te_2][UCl_6]$ and $[Hg_4As_2][UCl_6]$, *J. Solid State Chem.*, **2008**, *181*, 3189-3193.

(23) Janus, B.; Suski, W.; Blaise, A. Magnetic Properties of the Uranium Trichalcogenides. In *Crystalline Electric Field Effects in f-Electron Magnetism*: Guertin, R. P., Suski, W., Zolnierek, Z., Eds.; Springer: Boston, MA, **1982**; pp 539-544.

(24) Wells, D. M.; Ibers, J. A. The $[U_2I_{10}]^{2-}$ Anion: Synthesis and Structure of $[Ta_7(Se_2)_{14}][U_2I_{10}]_2$, *Z. Anorg. Allg. Chem.*, **2010**, *636*, 440-442.

(25) Choi, K.-S.; Patschke, R.; Billinge, S. J. L.; Waner, M. J.; Dantus, M.; Kanatzidis, M. G. Charge Density Wave Caused by Reducing $ThSe_3$ by One Electron. Superstructure and Short-Range Order in ATh_2Se_6 (A = K, Rb) Studied by X-ray Diffraction, Electron Diffraction, and Diffuse Scattering, *J. Am. Chem. Soc.*, **1998**, *120*, 10706-10714.

(26) Yao, J.; Wells, D. M.; Chan, G. H.; Zeng, H.-Y.; Ellis, D. E.; Duyne, R. P. V.; Ibers, J. A. Syntheses, Structures, Physical Poperties, and Electronic Properties of Some $AMUQ_3$ Compounds (A = Alkali Metal, M = Cu or Ag, Q = S or Se), *Inorg. Chem.*, **2008**, *47*, 6873-6879.

(27) Klepov, V. V.; Breton, L. S.; Pace, K. A.; Kocevski, V.; Besmann, T. M.; zur Loye, H.-C. Size-Driven Stability of Lanthanide Thiophosphates Grown from an Iodide Flux, *Inorg. Chem.*, **2019**, *58*, 6565-6573.

(28) Jin, G. B.; Choi, E. S.; Guertin, R. P.; Brooks, J. S.; Bray, T. H.; Booth, C. H.; Albrecht-Schmitt, T. E. Syntheses, Structure, Magnetism, and Optical Properties of the Ordered Mixed-Lanthanide Sulfides γ-LnLn'S_3 (Ln = La, Ce; Ln' = Er, Tm, Yb), *Chem. Mater.*, **2007**, *19*, 567-574.

(29) Gieck, C.; Tremel, W. Interlocking Inorganic Screw Helices: Synthesis, Structure, and Magnetism of the Novel Framework Uranium Orthothiophoshates $A_{11}U_7(PS_4)_{13}$ (A = K, Rb)., *Chemistry*, **2002**, *8*, 2980-2987.

(30) Neuhausen, C.; Hatscher, S. T.; Panthofer, M.; Urland, W.; Tremel, W. Comprehensive Uranium Thiophosphate Chemistry: Framework Compounds Based on Pseudotetrahedrally Coordinated Central Metal Atoms, *Z. Anorg. Allg. Chem.*, **2013**, *639*, 2836-2845.

(31) Klepov, V. V.; Juillerat, C. A.; Pace, K. A.; Morrison, G.; zur Loye, H.-C. "Soft" Alkali Bromide and Iodide Fluxes for Crystal Growth. *Front. Chem.* **2020**, *8*, 518.

(32) Wang, Y.; Yin, X.; Liu, W.; Xie, J.; Chen, J.; Silver, M. A.; Sheng, D.; Chen, L.; Diwu, J.; Liu, N.; Chai, Z.; Albrecht-Schmitt, T. E.; Wang, S. Emergence of Uranium as a Distinct Metal Center for Building Intrinsic X-ray Scintillators, *Angew. Chem. Int. Ed. Engl.*, **2018**, 57, 7883-7887.

(33) Gui, D.; Duan, W.; Shu, J.; Zhai, F.; Wang, N.; Wang, X.; Xie, J.; Li, H.; Chen, L.; Diwu, J.; Chai, Z.; Wang, S. Persistent Superprotonic Conductivity in the Order of 10^{-1} S•cm^{-1} Achieved Through Thermally Induced Structural Transformation of a Uranyl Coordination Polymer, *CCS Chem.*, **2019**, 1, 197-206.

(34) Daoudi, A.; Noel, H. Synthese, structure cristalline et proprietes magnetiques du seleniure ternaire d'uranium et de palladium: $PdUSe_3$, *J. of the Less Common Met.*, **1989**, *153*, 293-298.

(35) Daoudi, A.; Noel, H. Synthesis, crystal structure and magnetic properties of new ternary uranium chalcogenides: $RuUS_3$ and $RhUS_3$, *Inorganica Chim. Acta*, **1987**, *140*, 93-95.

(36) Noel, H.; Potel, M.; Padiou, J. Structure cristalline de CrU_8S_{17}, *Acta. Crystallogr. B*, **1975**, *31*, 2634-2637.

(37) Cody, J. A.; Ibers, J. A. Uranium Tellurides: New One- and Two-Dimensional Compounds $CsUTe_6$, $CsTiUTe_5$, $Cs_8Hf_5UTe_{30.6}$, and $CsCuUTe_3$, *Inorg. Chem.*, **1995**, *34*, 3165-3172.

(38) Bugaris, D. E.; Wells, D. M.; Yao, J.; Skanthakumar, S.; Haire, R. G.; Soderholm, L.; Ibers, J. A. Dichalcogenide Bonding in Seven Alkali-Metal Actinide Chalcogenides of the KTh_2Se_6 Structure Type., *Inorg. Chem.*, **2010**, *49*, 8381-8388.

(39) Mesbah, A.; Ibers, J. A. Syntheses and crystal structures of three barium uranium sulfides, *J. Solid State Chem.*, **2013**, *199*, 253-257.

(40) Ward, M. D.; Ibers, J. A. The Synthesis and Crystal Structure of $U_7O_2Se_{12}$, *Z. Anorg. Allg. Chem.*, **2014**, *640*, 1585-1588.

(41) Mesbah, A.; Prakash, J.; Beard, J. C.; Pozzi, E. A.; Tarasenko, M. S.; Lebegue, S.; Malliakas, C. D.; Duyne, R. P. V.; Ibers, J. A. Positional Flexibility: Synthesis and Characterization of Six Uranium Chalcogenides Related to the 2H Hexagonal Perovskite Family, *Inorg. Chem.*, **2015**, *54*, 2851-2857.

(42) Prakash, J.; Tarasenko, M. S.; Mesbah, A.; Lebegue, S.; Malliakas, C. D.; Ibers, J. A. Synthesis, Crystal Structure, Theoretical, and Resistivity Study of $BaUSe_3$., *Inorg. Chem.*, **2016**, *55*, 7734-7738.

(43) Mesbah, A.; Prakash, J.; Beard, J. C.; Lebegue, S.; Malliakas, C. D.; Ibers, J. A. Four new actinide chalcogenides $Ba_2Cu_4USe_6$, $Ba_2Cu_2ThSe_5$, $Ba_2Cu_2USe_5$, and $Sr_2Cu_2US_5$: Crystal Structures and Physical Properties, *Inorg. Chem.*, **2015**, *54*, 9138-9145.

(44) Ippolitova, E. A.; Dunaeva, K. M.; Mitrofanova, N. D. Investigation of the Oxidation Process of Uranium Disulfide. In *Investigations in the Field of Uranium Chemistry*: Spitsyn, V. I., Ed.; U.S. Atomic Energy Commission, **1964**; pp 245-259.

(45) Wu, L.-M.; Seo, D.-K. New Solid-Gas Metathetical Synthesis of Binary Metal Polysulfides and Sulfides at Intermediate Temperatures: Utilization of Boron Sulfides, *J. Am. Chem. Soc.*, **2004**, *126*, 4676-4681.

(46) Zhang, M.-J.; Jiang, X.-M.; Zhou, L.-J.; Guo, G.-C. Two phases of Ga_2S_3: promising infrared second-order nonlinear optical materials with very high laser induced damage thresholds, *J. Mater. Chem. C*, **2013**, *1*, 4754.

(47) Guo, S.-P.; Chi, Y.; Xue, H.-G. $Sm_3S_3BO_3$: The First Sulfide Borate without S-O and B-S Bonds., *Inorg. Chem.*, **2015**, *54*, 11052-11054.

(48) Guo, S.; Guo, G.; Huang, J. Syntheses, structures and properties of five chiral quaternary sulfides, $Al_xLn_3(Si_yAl_{1-y})S_7$ (Ln = Y, Gd, Dy) and $In_{0.33}Sm_3SiS_7$, *Science in China Series B: Chemistry*, **2009**, *52*, 1609-1615.

(49) Huang, Y.-Z.; Chen, L.; Wu, L.-M. Crystalline Nanowires of Ln_2O_2S, $Ln_2O_2S_2$, LnS_2 (Ln = La, Nd), and $La_2O_2S:Eu^{3+}$. Conversions via the Boron-Sulfur Method That Preserve Shape, *Cryst. Growth Des.*, **2008**, *8*, 739-743.

(50) Jeon, K.-W.; Seo, D.-K. Concomitant Thionation and Reduction of Graphene Oxide Through Solid/Gas Metathetical Sulfidation Reactions at High Temperatures, *Phosphorus, Sulfur, and Silicon and the Related Elements*, **2014**, *189*, 721-737.

(51) Malliakas, C. D.; Yao, J.; Wells, D. M.; Jin, G. B.; Skanthakumar, S.; Choi, E. S.; Balasubramanian, M.; Soderholm, L.; Ellis, D. E.; Kanatzidis, M. G.; Ibers, J. A. Oxidation State of Uranium in $A_6Cu_{12}U_2S_{15}$ (A = K, Rb, Cs) Compounds, *Inorg. Chem.*, **2012**, *51*, 6153-6163.

(52) Sutorik, A. C.; Kanatzidis, M. G. Reactions of Lanthanides and Actinides in Molten Alkali Metal/Polychalcogenide Fluxes at Intermediate Temperatures (250-600 ºC), *Chem. Mater.*, **1997**, *9*, 387-398.

(53) Suski, W.; Gibinski, T.; Wojakowski, A.; Czopnik, A. The crystal structure and magnetic and electrical properties of β-US_2, *phys. stat. sol. (a)*, **1972**, *9*, 653.

(54) Saal, J. E.; Kirklin, S.; Aykol, M.; Meredig, B.; Wolverton, C. Materials Design and Discovery with High-Throughput Density Functional Theory: The Open Quantum Materials Database (OQMD), *JOM*, **2013**, *65*, 1501-1509.

(55) Kirklin, S.; Saal, J. E.; Meredig, B.; Thompson, A.; Doak, J. W.; Aykol, M.; Ruhl, S.; Wolverton, C. The Open Quantum Materials Database (OQMD): assessing the accuracy of DFT formation energies, *npj Computational Materials*, **2015**, *1*, 15010.

(56) Jansen, M. Conceptual Inorganic Materials Discovery - A Road Map, *Advanced Materials*, **2015**, *27*, 3229-3242.

(57) Klepov, V. V.; Smith, M. D.; zur Loye, H.-C. Targeted Synthesis of Uranium(IV) Thiosilicates., *Inorg. Chem.*, **2019**, *58*, 8275-8278.

(58) Sheldrick, W. S. Polychalcogenides. In *Handbook of Chalcogen Chemistry*: Devillanova, F., Du Mont, W., Eds.; The Royal Society of Chemistry, **2007**; pp 543-557.

(59) Noel, H.; Padiou, J.; Prigent, J. Mixed Uranium and Transition Element Sulfides, *C. R. Acad. Sc. Paris*, **1971**, *272*, 206-208.

(60) Ward, M. D.; Ibers, J. A. Nickel(II) uranium(IV) trisulfide., *Acta Crystallogr. Sect. E: Struct. Rep. Online*, **2014**, *70*, i4.

(61) Murphy, G. L.; Kegler, P.; Zhang, Y.; Zhang, Z.; Alekseev, E. V.; Jonge, M. D. D.; Kennedy, B. J. High-Pressure Synthesis,

Structural, and Spectroscopic Studies of the Ni—U—O System, *Inorg. Chem.*, **2018**, *57*, 13847-13858.

(62) Chenevier, B.; Wolfers, P.; Bacmann, M.; Noel, H. $CoUS_3$-Proprietes et structure magnetiques, *C. R. Acad. Sc. Paris*, **1981**, *293*, 649-652.

(63) Bugaris, D. E.; zur Loye, H.-C. Materials Discovery by Flux Crystal Growth: Quaternary and Higher Order Oxides, *Angew. Chem. Int. Ed.*, **2012**, *51*, 3780-3811.

(64) Noel, H.; Prigent, J. U_3S_5: A mixed valence uranium sulfide. Magnetic susceptibility of thorium and lanthanides isomorphous derivatives, *Physica B+C*, **1980**, *102B*, 372-379.

(65) Grønvold, F.; Haraldsen, H.; Thurmann-Moe, T.; Tufte, T. Uranium chalcogenides—I structural and magnetic properties of sulphides and selenides in the range $UX_{1.5}$ to UX_3, *J. Inorg. Nucl. Chem.*, **1968**, *30*, 2117-2125.

(66) Noel, H.; Marouille, J. Y. L. E. Crystal structure and properties of the uranium chalcogenides α-US_2 and α-USe_2, *J. Solid State Chem.*, **1984**, *52*, 197-202.

(67) Klepov, V. V.; zur Loye, H.-C. Complex Topologies from Simple Building Blocks: Uranium(IV) Thiophosphates, *Inorg. Chem.*, **2018**, *57*, 11175-11183.

(68) Simon, A.; Peters, K.; Peters, E.-M.; Hahn, H. Darstellung und Kristallstruktur von ZrP_2S_6 und ThP_2S_6, *Z. Anorg. Allg. Chem.*, **1982**, *491*, 295-300.

(69) Chan, B. C.; Hess, R. F.; Feng, P. L.; Abney, K. D.; Dorhout, P. K. Synthesis and Characterization of Two Quaternary Thorium Chalcophosphates: $Cs_4Th_2P_6S_{18}$ and $Rb_7Th_2P_6Se_{21}$, *Inorg. Chem.*, **2005**, *44*, 2106-2113.

(70) Mesbah, A.; Prakash, J.; Beard, J. C.; Lebegue, S.; Malliakas, C. D.; Ibers, J. A. Synthesis, Crystal Structures, Optical and Theoretical Studies of the Actinide Thiophosphates $SrU(PS_4)_2$, $BaU(PS_4)_2$, and $SrTh(PS_4)_2$, *Inorg. Chem.*, **2015**, *54*, 2970-2975.

(71) Hess, R. F.; Abney, K. D.; Burris, J. L.; Hochheimer, H. D.; Dorhout, P. K. Synthesis and Characterization of Six New Quaternary Actinide Thiophosphate Compounds: $Cs_8U_5(P_3S_{10})_2(PS_4)_6$, $K_{10}Th_3(P_2S_7)_4(PS_4)_2$, and $A_5An(PS_4)_3$, (A = K, Rb, Cs; An = U, Th), *Inorg. Chem.*, **2001**, *40*, 2851-2859.

(72) Ward, M. D.; Lee, M.; Choi, E. S.; Ibers, J. A. Synthesis and characterization of the quaternary scandium uranium selenide $CsScUSe_3(Se_2)$, *J. Solid State Chem.*, **2015**, *226*, 307-311.

(73) Mesbah, A.; Prakash, J.; Lebegue, S.; Stojko, W.; Ibers, J. A. Syntheses, crystal structures, and electronic properties of $Ba_8Si_2US_{14}$ and $Ba_8SiFeUS_{14}$, *Solid State Sci.*, **2015**, *48*, 120-124.

(74) Mesbah, A.; Prakash, J.; Beard, J. C.; Malliakas, C. D.; Lebegue, S.; Ibers, J. A. Syntheses, modulated crystal structures of $Ba_{6-2x}U_{2+x}Ag_4Se_{12}$ (x = 0 and 0.5), and crystal structure and spectroscopy of $Sr_4Th_{2.78}Cu_4S_{12}$, *J. Solid State Chem.*, **2018**, *268*, 30-35.

(75) Mesbah, A.; Ringe, E.; Lebegue, S.; Duyne, R. P. V.; Ibers, J. A. $Ba_2An(S_2)_2S_2$ (An = U, Th): Syntheses, Structures, Optical, and Electronic Properties, *Inorg. Chem.*, **2012**, *51*, 13390-13395.

(76) Mesbah, A.; Stojko, W.; Lebegue, S.; Malliakas, C. D.; Frazer, L.; Ibers, J. A. The U^{5+} compound $Ba_9Ag_{10}U_4S_{24}$: Synthesis, structure, and electronic properties, *J. Solid State Chem.*, **2015**, *221*, 398-404.

(77) Ward, M. D.; Mesbah, A.; Minasian, S. G.; Shuh, D. K.; Tyliszczak, T.; Lee, M.; Choi, E. S.; Lebegue, S.; Ibers, J. A. Synthesis and Characterization of Eight Compounds of the MU_8Q_{17} Family: ScU_8S_{17}, CoU_8S_{17}, NiU_8S_{17}, TiU_8Se_{17}, VU_8Se_{17}, CrU_8Se_{17}, CoU_8Se_{17}, and NiU_8Se_{17}., *Inorg. Chem.*, **2014**, *53*, 6920-6927.

(78) Brown, I. D. Bond Valence Parameters, https://www.iucr.org/resources/data/datasets/bond-valence-parameters, (June 10, 2020), IUCr.

TOC graphic

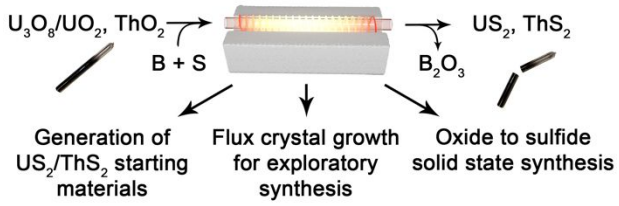
U_3O_8/UO_2, ThO_2
B + S
US_2, ThS_2
B_2O_3
Generation of US_2/ThS_2 starting materials
Flux crystal growth for exploratory synthesis
Oxide to sulfide solid state synthesis